# 3-D network model and its parameter calibration

LIU Xiaoyu (刘晓宇), LIANG Naigang (梁乃刚) & LI Min (李 敏)

State Key Laboratory of Nonlinear Mechanics, Institute of Mechanics, Chinese Academy of Sciences, Beijing 100080, China

Correspondence should be addressed to Liu Xiaoyu (email: liuxy@lnm.imech.ac.cn)

Received December 28, 2001

**Abstract** A material model, whose framework is parallel spring-bundles oriented in 3-D space, is proposed. Based on a discussion of the discrete schemes and optimum discretization of the solid angles, a 3-D network cell consisted of one-dimensional components is developed with its geometrical and physical parameters calibrated. It is proved that the 3-D network model is able to exactly simulate materials with arbitrary Poisson ratio from 0 to 1/2, breaking through the limit that the previous models in the literature are only suitable for materials with Poisson ratio from 0 to 1/3. A simplified model is also proposed to realize high computation accuracy within low computation cost. Examples demonstrate that the 3-D network model has particular superiority in the simulation of short-fiber reinforced composites.

**Keywords: strain energy stiffness modulus, orientation component, network model, poisson ratio.**

Network models, also called lattice model in some references, have been applied to many fields over the past forty years. Before computer techniques were widely used, facing to large engineering structures consisting of truss elements, one used discrete models for structural analysis[1,2]. In the middle and the late 1980s, with the development of computer techniques, theoretical physicists introduced a few 2-D network models to study the universal statistical laws of disorder media during brittle fracture processes[3]. In the 1990s, network models played an important role in the prediction of mechanical performance and investigation of damage evolution of materials such as concrete[4], ceramics[5], particle reinforced composites[6] and short-fiber reinforced composites[7–9].

For 2-D network models, their physical and geometrical parameters are able to be uniquely determined in terms of the spatial symmetry and the equivalence of strain energy between network and continuum cells[10]. Moreover, it was proved that as the size of 2-D network cell goes smaller and smaller, the limitation of the predicted deformation field satisfies Lame's equations in continuum mechanics[7]. However, there are few theoretical studies and applications on 3-D network models up to now. The reason may be that the complex geometry of 3-D network models makes it impossible to directly calibrate the geometrical and physical parameters of components in terms of the spatial symmetry.

Ostojastarzewski[10] pointed out that network method is, in principle, based on the atomic lattice model of materials. Directly starting from the interaction between atoms in a material, a material model is drawn out and the discrete schemes are discussed. A 3-D network model is con-

structed with its geometrical and physical parameters calibrated. A simplified model is also proposed, and its computational accuracy is analyzed. Finally, the superiority and potentiality that the 3-D network model simulates short-fiber reinforced composites is discussed.

## 1 Material model based on interaction between atoms

### 1.1 Strain energy of material cell and spring-bundle material model

At the microscopic scale, a macroscopic material cell includes infinite atoms, and the strain energy of the material cell is determined by the interaction between atoms. Based on the embedded-atom method[11], the strain energy of a material cell is given in terms of an embedding energy accounting for the interaction between the nuclei and surrounding electron gas, and a second term accounting for the self-interaction of the nuclei, namely,

$$W = \sum_i [\Phi_i + U_i(\rho_i)], \tag{1}$$

where $i$ runs over all atoms in the material cell, $\Phi_i$ is the total interaction energy of atom $i$ with all other nuclei, $\rho_i$ is the ambient electron density at atom $i$, $U_i$ is the energy required to embed atom $i$ into electron density $\rho_i$.

By virtue of eq. (1), a real material cell can be regarded as a composite of two simple materials undergoing the same deformation and undertaking together the loading subject to the real material. The strain energy of the first simple material is given by the first term on the right side of eq. (1), and the one of the second simple material is given by the second term.

In the first simple material, the interactions between an atom, such as atom $A$ in fig. 1, and other atoms are represented by springs. In the coordinate system shown in fig. 2, denote the direction cosines in direction $(\theta, \phi)$ as

$$n_1 = \sin\phi\cos\theta, \quad n_2 = \sin\phi\sin\theta, \quad n_3 = \cos\phi, \tag{2}$$

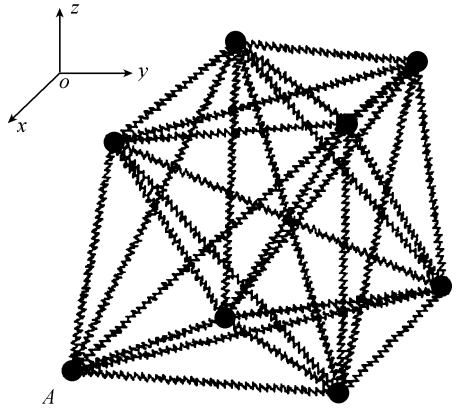


Fig. 1. Schematic illustrating a spring network.

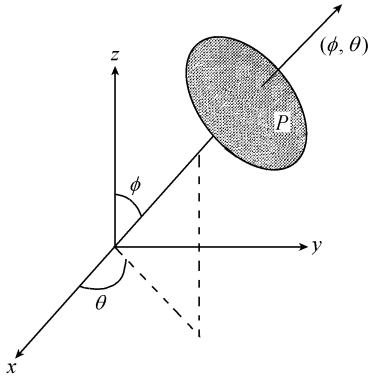


Fig. 2. Coordinate system and unit area in $(\theta, \phi)$ direction.

the solid angle in a neighborhood of direction $(\theta,\phi)$ is expressed as $\Delta\Omega=\sin\phi\Delta\phi\Delta\theta$. Suppose there is a unit area cross section $P$ perpendicular to direction $(\theta,\phi)$ in fig. 2, whose scale is far much larger than the average distance between atoms. When the material cell is subject to a macroscopic strain increment $\Delta\varepsilon$ in direction $(\theta,\phi)$, denote the result force exerted on area $P$ from all the springs oriented in $\Delta\Omega$ as $\Delta F$. The elastic modulus of material cell in direction $(\theta,\phi)$ can be defined as $H(\theta,\phi)$ and

$$H(\theta,\phi)\Delta\Omega=\frac{\Delta F}{\Delta\varepsilon}. \tag{3}$$

Therefore, under macroscopic strain $\varepsilon_{ij}$, the total strain energy of all springs oriented in $\Delta\Omega$ in unit volume material will be

$$\Delta W_1(\theta,\phi)=\frac{1}{2}H(\theta,\phi)n_i(\theta,\phi)n_j(\theta,\phi)n_r(\theta,\phi)n_s(\theta,\phi)\varepsilon_{ij}\varepsilon_{rs}\sin\phi\Delta\phi\Delta\theta. \tag{4}$$

With direction $n_i$ ($i$ = 1,2,3) going over the above half solid angle ($z\geqslant 0$), the total strain energy of unit volume material

$$W_1=\frac{1}{2}\varepsilon_{ij}\varepsilon_{rs}\int_0^{\pi/2}\sin\phi\left[\int_0^{2\pi}H(\theta,\phi)n_i(\theta,\phi)n_j(\theta,\phi)n_r(\theta,\phi)n_s(\theta,\phi)d\theta\right]d\phi. \tag{5}$$

For an isotropic material, the elastic moudlus $H$ is constant. Then eq. (5) becomes

$$W_1=\frac{\pi}{15}H\varepsilon_{ij}\varepsilon_{rs}(\delta_{ij}\delta_{rs}+\delta_{ir}\delta_{js}+\delta_{is}\delta_{jr}), \tag{6}$$

where $\delta_{ij}$ is Kronecker symbol.

The strain energy of the second simple material is only dependent on the volume deformation. Under macroscopic strain $\varepsilon_{ij}$, the strain energy is written as

$$W_2=\frac{1}{2}\rho_c\delta_{ij}\delta_{rs}\varepsilon_{ij}\varepsilon_{rs}, \tag{7}$$

where $\rho_c$ is the volume modulus.

### 1.2 Discretization by orientation

For the first simple material, its strain energy can be discretized by orientation. Then eq. (5) can be written as

$$W_1=\frac{1}{2}\varepsilon_{ij}\varepsilon_{rs}\iint_{\Omega}H(\Omega)n_i(\Omega)n_j(\Omega)n_r(\Omega)n_s(\Omega)d\Omega, \tag{8}$$

where $\Omega$ is the solid angle represented by orientation $n_i(\Omega)$. Divide the above half ($0\leqslant\phi\leqslant\pi/2$) into $M$ solid angles, and the representative direction of the $\alpha$th solid angle is $n^{(\alpha)}$, then eq. (8) becomes

$$W_1 = \sum_{\alpha=1}^{M} \Delta W^{(\alpha)} = \frac{1}{2}\varepsilon_{ij}\varepsilon_{rs}\sum_{\alpha=1}^{M} H^{(\alpha)} n_i^{(\alpha)} n_j^{(\alpha)} n_r^{(\alpha)} n_s^{(\alpha)} \Delta\Omega^{(\alpha)}. \tag{9}$$

On the other hand, for a parallel spring-bundles with orientation $n_i^{(\alpha)}$ and stiffness modulus $K^{(\alpha)}$, its unit volume strain energy

$$W^{(\alpha)} = \frac{1}{2}\varepsilon_{ij}\varepsilon_{rs} K^{(\alpha)} n_i^{(\alpha)} n_j^{(\alpha)} n_r^{(\alpha)} n_s^{(\alpha)}. \tag{10}$$

Compared with eqs. (9) and (10), material cell is composed of *M* groups of parallel springs, each of which has stiffness modulus

$$K_0^{(\alpha)} = H^{(\alpha)} \Delta\Omega^{(\alpha)}. \tag{11}$$

1.3 Representative directions of discrete solid angles

To ensure the computational accuracy, it is necessary to reasonably choose the sum of discrete solid angles *M* and the representative orientation of each discrete solid angle $n^{(\alpha)}$.

Thinking of the symmetry in the 3-D rectangular coordinate system, fig. 3(a)—(d) shows several possible discrete manners in the stereographic projection. In fig. 3(a), there are 9 representative directions with direction numbers [1,0,0], [0,1,0], [0,0,1], [1,1,0], [1,0,1], [0,1,1], [1, $\bar{1}$ ,0], [ $\bar{1}$ ,0,1] and [0, $\bar{1}$ ,1], respectively ( $\bar{1}$ represents −1, similarly hereinafter). Fig. 3(b) shows a manner of 7 representative directions with direction numbers [1,0,0], [0,1,0], [0,0,1], [1,1,1], [ $\bar{1}$ ,1,1], [1, $\bar{1}$ ,1] and [ $\bar{1}$ , $\bar{1}$ ,1], respectively. Fig. 3(c) shows a manner of 13 representative directions with direction numbers [1,0,0], [0,1,0], [0,0,1], [1,1,0], [1,0,1], [0,1,1], [1, $\bar{1}$ ,0], [ $\bar{1}$ ,0,1], [0, $\bar{1}$ ,1], [1,1,1], [ $\bar{1}$ ,1,1], [1, $\bar{1}$ ,1] and [ $\bar{1}$ , $\bar{1}$ ,1], respectively. Fig. 3(d) is a scheme with 37 representative directions. The direction numbers of five typical directions are [1,0,0], [1,1,0], [1,1,1], [2,1,0] and [2,1,1], respectively. With the increase of the number of the discrete solid angles, the orientation deviation among discrete solid angles decreases and the accuracy of discrete approximation increases. Of course, the increase of the sum of discrete solid angles leads to the increase of computational cost. Numerical investigation indicates that the discrete manner shown in fig. 3(c) is a good compromise in consideration of the accuracy and cost.

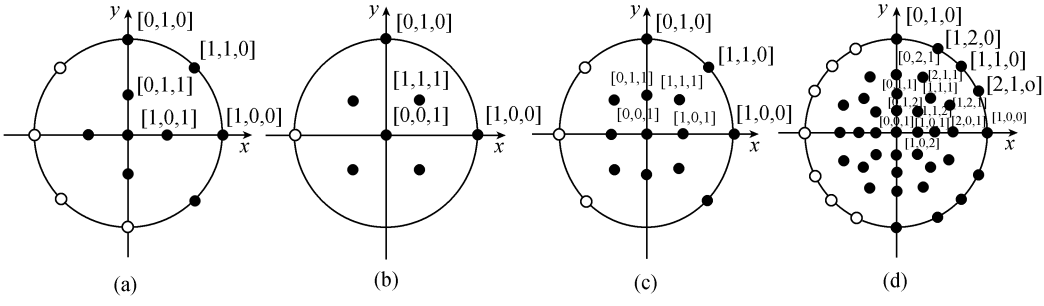


Fig. 3. Stereographic projections of representative directions in four discrete manners.

Without losing generality, the discrete manner shown in fig. 3(c) will be employed and eq. (8) is discretized by 13 directions. Then eq. (9) becomes

$$W_1 = \frac{1}{2}\varepsilon_{ij}\varepsilon_{rs}\sum_{\alpha=1}^{13} H^{(\alpha)} n_i^{(\alpha)} n_j^{(\alpha)} n_r^{(\alpha)} n_s^{(\alpha)} \Delta\Omega^{(\alpha)}. \tag{12}$$

1.4 Determination of discrete solid angles

The representative directions shown in fig. 3(c) are divided into three groups. The representative directions in the first group are [1,0,0], [0,1,0] and [0,0,1]; the second group are [1,1,0], [1,0,1], [0,1,1], [1, $\bar{1}$ ,0], [ $\bar{1}$ ,0,1] and [0, $\bar{1}$ ,1]; the third group are [1,1,1], [ $\bar{1}$ ,1,1], [1, $\bar{1}$ ,1], [ $\bar{1}$ , $\bar{1}$ ,1]. Denote the three groups' solid angles are $\Delta\Omega^{(1)}$, $\Delta\Omega^{(2)}$ and $\Delta\Omega^{(3)}$, respectively. Then, for an isotropic material, eq. (12) becomes

$$\begin{aligned} W_1 = \frac{1}{2}H\varepsilon_{ij}\varepsilon_{rs}\{&\Delta\Omega^{(1)}(\delta_{i1}\delta_{j1}\delta_{r1}\delta_{s1}+\delta_{i2}\delta_{j2}\delta_{r2}\delta_{s2}+\delta_{i3}\delta_{j3}\delta_{r3}\delta_{s3}) \\ &+\frac{\Delta\Omega^{(2)}}{2}[(\delta_{ij}\delta_{rs}+\delta_{ir}\delta_{js}+\delta_{is}\delta_{jr})-(\delta_{i1}\delta_{j1}\delta_{r1}\delta_{s1}+\delta_{i2}\delta_{j2}\delta_{r2}\delta_{s2}+\delta_{i3}\delta_{j3}\delta_{r3}\delta_{s3})] \\ &+\frac{\Delta\Omega^{(3)}}{9}[4(\delta_{ij}\delta_{rs}+\delta_{ir}\delta_{js}+\delta_{is}\delta_{jr})-8(\delta_{i1}\delta_{j1}\delta_{r1}\delta_{s1}+\delta_{i2}\delta_{j2}\delta_{r2}\delta_{s2}+\delta_{i3}\delta_{j3}\delta_{r3}\delta_{s3})]\}. \end{aligned} \tag{13}$$

Comparing eq. (6) with eq. (13) gives

$$\Delta\Omega^{(1)} + \Delta\Omega^{(2)} + \frac{4}{9}\Delta\Omega^{(3)} = \frac{2}{5}\pi \tag{14}$$

and

$$\frac{1}{2}\Delta\Omega^{(2)} + \frac{4}{9}\Delta\Omega^{(3)} = \frac{2}{15}\pi. \tag{15}$$

As is well known, the smaller the size-difference among these discrete solid angles, the higher the discrete accuracy. Therefore, the optimum discrete scheme makes

$$\chi = \max(\Delta\Omega^{(1)}, \Delta\Omega^{(2)}, \Delta\Omega^{(3)}) / \min(\Delta\Omega^{(1)}, \Delta\Omega^{(2)}, \Delta\Omega^{(3)}) \tag{16}$$

reach its minimum. Letting $\xi = \Delta\Omega^{(3)} / \Delta\Omega^{(2)}$ and substituting it into eq. (14) and eq. (15) give

$$\Delta\Omega^{(1)} : \Delta\Omega^{(2)} : \Delta\Omega^{(3)} = \left(\frac{8}{9}\xi + \frac{1}{2}\right) : 1 : \xi. \tag{17}$$

The dependence of $\chi$ on $\xi$ is depicted in fig. 4. When $\xi$ = 1, eq. (17) reaches its minimum. Letting $\Delta\Omega^{(2)} = \Delta\Omega^{(3)}$ and combining eq. (14) and eq. (15) give

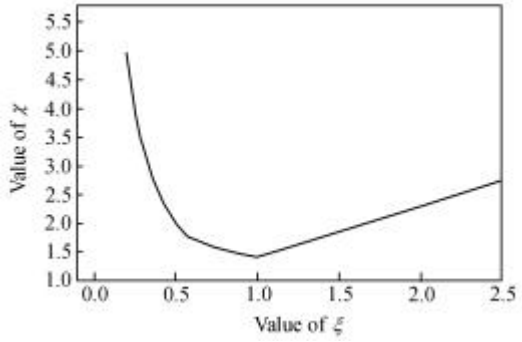


Fig. 4. $\chi$~$\xi$ curve.

$$\Delta\Omega^{(1)} = \frac{10}{51}\pi, \quad \Delta\Omega^{(2)} = \frac{12}{85}\pi, \quad \Delta\Omega^{(3)} = \frac{12}{85}\pi. \tag{18}$$

The discrete solid angles for other discrete manners can also be determined analogously.

## 2 3-D network model

Based on the discrete manner shown in fig. 3(c), the material cell is modeled by parallel spring-bundles oriented in the 13 directions, and the stiffness moduli of the spring-bundles are determined by eq. (13). Provided that a spring-bundle can be represented by a 1-D component with the same orientation and stiffness modulus, a 3-D network model cell shown in fig. 5(a) is constructed.

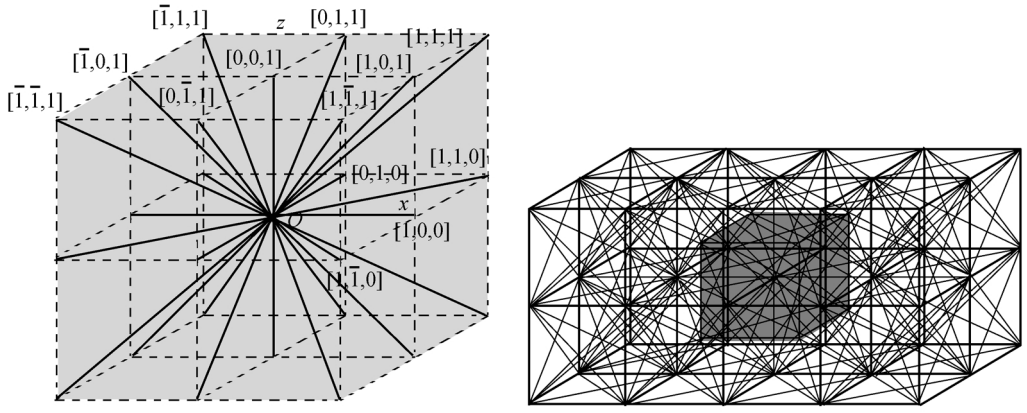


Fig. 5. Unit 3-D network cell (a) and a discrete material volume (b).

For a regular hexahedron network cell with volume $a^3$, the length of the components in the three groups is $a/2$, $a\sqrt{2}/2$ and $a\sqrt{3}/2$, respectively. According to the length and corresponding discrete solid angle, the stiffness of the $\alpha$th component in the network cell

$$k^{(\alpha)} = a^3 H^{(\alpha)} \Delta\Omega^{(\alpha)} / (L^{(\alpha)})^2 . \tag{19}$$

Therefore, the stiffness $k^{(i)}$ ($i$ = 1, 2, 3) of the components in the three groups satisfies

$$k^{(1)} : k^{(2)} : k^{(3)} = 25 : 9 : 6. \tag{20}$$

## 3 Parameter calibration of 3-D network model

### 3.1 Strain energy of network cell

When network cell simulates a material, the strain energy of the network can be written as

$$U = \frac{1}{2} \sum_{\langle \alpha,\beta \rangle} k^{(\alpha,\beta)} [(\boldsymbol{u}^{(\alpha)} - \boldsymbol{u}^{(\beta)}) \cdot \boldsymbol{n}^{(\alpha,\beta)}]^2, \tag{21}$$

where $\alpha$ and $\beta$ are the serial number of the nodes; $\langle \alpha,\beta \rangle$ sums over all the components; $\boldsymbol{u}^{(\alpha)}$ and $\boldsymbol{u}^{(\beta)}$ are the displacements of nodes $\alpha$ and $\beta$, respectively; $\boldsymbol{n}^{(\alpha,\beta)}$ is the unit vector from nodes $\alpha$ to $\beta$; $k^{(\alpha,\beta)}$ is the tensile stiffness of the component, one of the $k^{(i)}$, respectively.

Under pure shear deformation ($u_1 = \gamma x_3$, $u_2 = 0$, $u_3 = \gamma x_1$), the strain energy of network cell with side $a$ shown in fig. 5(a)

$$U_\gamma = \left( k^{(2)} + \frac{4}{3} k^{(3)} \right) a^2 \gamma^2. \tag{22}$$

Under pure dilatation ( $u_1 = \eta x_1, \quad u_2 = \eta x_2, \quad u_3 = \eta x_3$ ), the strain energy of network cell

$$U_e = \left( \frac{3}{4} k^{(1)} + 3k^{(2)} + 3k^{(3)} \right) a^2 \eta^2. \tag{23}$$

3.2 Balance and objectivity requirements

By differentiating the energy $U$ with respect to $\boldsymbol{u}^{(\alpha)}$, the resultant force exerted on node $\alpha$ can be obtained, which vanishes at equilibrium, so that

$$F_\alpha = -\frac{\partial U}{\partial u^{(\alpha)}} = \sum_{\substack{\beta \\ \langle \alpha, \beta \rangle}} k^{(\alpha,\beta)} \{ [(\boldsymbol{u}^{(\beta)} - \boldsymbol{u}^{(\alpha)}) \cdot \boldsymbol{n}^{(\alpha,\beta)}] \boldsymbol{n}^{(\alpha,\beta)} \} = 0. \tag{24}$$

When the size of the network cell gets smaller and smaller, node $\beta$ approaches to node $\alpha$, $\boldsymbol{u}^{(\beta)}$ can be expanded in Taylor series around node $\alpha$ up to the second order as

$$u_i^{(\beta)} - u_i^{(\alpha)} = L^{(\alpha,\beta)} \frac{\partial u_i}{\partial x_s} n_s^{(\alpha,\beta)} + \frac{1}{2} [L^{(\alpha,\beta)}]^2 \frac{\partial^2 u_i}{\partial x_s \partial x_t} n_s^{(\alpha,\beta)} n_t^{(\alpha,\beta)} \quad (i = 1, 2, 3), \tag{25}$$

where $L^{(\alpha,\beta)}$ and $n_s^{(\alpha,\beta)}$ are the length and direction cosine of the component connecting nodes $\alpha$ and $\beta$, respectively.

Substituting eq. (25) into eq. (24), the balance equations require the stiffnesses of components satisfy

$$\begin{aligned} & a^2 \left[ \left( k^{(1)} - k^{(2)} - \frac{8}{3} k^{(3)} \right) \right] \left( \delta_{i1} \frac{\partial^2 u_1}{\partial x_1 \partial x_1} + \delta_{i2} \frac{\partial^2 u_2}{\partial x_2 \partial x_2} \delta_{i3} \frac{\partial^2 u_3}{\partial x_3 \partial x_3} \right) \\ & + a^2 \left( 2k^{(2)} + \frac{8}{3} k^{(3)} \right) \frac{\partial^2 u_k}{\partial x_i \partial x_k} + \left( k^{(2)} + \frac{4}{3} k^{(3)} \right) \frac{\partial^2 u_i}{\partial x_k \partial x_k} = 0. \end{aligned} \tag{26}$$

On the other hand, the equilibrium equations of material cell expressed by displace are

$$(\lambda - \rho_c + \mu) \frac{\partial^2 u_k}{\partial x_i \partial x_k} + \mu \frac{\partial^2 u_i}{\partial x_k \partial x_k} = 0, \tag{27}$$

where $\lambda$ and $\mu$ are the Lame coefficients of the material. Comparing eq. (26) with eq. (27), the stiffness of the components in network cell satisfies

$$k^{(1)} - k^{(2)} - \frac{8}{3} k^{(3)} = 0, \tag{28}$$

$$\frac{2k^{(2)} + \frac{8}{3} k^{(3)}}{k^{(2)} + \frac{4}{3} k^{(3)}} = \frac{\lambda - \rho_c + \mu}{\mu}. \tag{29}$$

It can be verified that eq. (28) is independent of the coordinate system chosen, namely, the objec-

tivity requirement. Obviously, the stiffness in eq. (20) satisfies eq. (28). Meanwhile, by virtue of eq. (20) and eq. (29), the volume modulus of the second simple material

$$\rho_c = \lambda - \mu. \tag{30}$$

3.3 Shear modulus requirement and parameter calibration

Eq. (22) indicates that in order to simulate the shear modulus requirement of material cell, the stiffness of the components must satisfy

$$k^{(2)} + \frac{4}{3}k^{(3)} = 2a\mu. \tag{31}$$

Then when satisfying the discretization requirement expression eq. (20) and the shear modulus requirement expression eq. (31), the stiffness of the components

$$k^{(1)} = \frac{50}{17}\mu a, \quad k^{(2)} = \frac{18}{17}\mu a, \quad k^{(3)} = \frac{12}{17}\mu a. \tag{32}$$

It is verified that the components' stiffness calibrated satisfies the volume modulus requirement of material cell, namely

$$\left(\frac{3}{4}k^{(1)} + 3k^{(2)} + 3k^{(3)}\right)a^2 = \frac{3}{2}(3\lambda + 2\mu)a^3 - \frac{9}{2}\rho_c a^3, \tag{33}$$

and satisfies the tensile modulus requirement, namely

$$\left(\frac{1}{4}k^{(1)} + \frac{1}{2}k^{(2)} + \frac{1}{3}k^{(3)}\right)a^2 = \left(\frac{1}{2}\lambda + \mu\right)a^3 - \frac{1}{2}\rho_c a^3. \tag{34}$$

## 4 Simplified 3-D network model

When the Poisson ratio = 1/4, $\lambda = \mu$, and $\rho_c = 0$, the strain energy of the second simple material is zero. Because the Poisson ratio of most engineering materials is near 1/4, $\rho_c << k^{(1)}, k^{(2)}, k^{(3)}$, then the effect of the second simple material can be neglectable. Moreover, in many cases, the effect of hydrostatic stress on the material behavior is not the major factor of problems. In this case, neglecting $\rho_c$ and letting

$$\mu = \frac{8 + 8\nu'}{9 + 4\nu'}\mu', \quad E = \frac{10}{9 + 4\nu'}E', \tag{35}$$

and

$$k^{(1)} = \frac{400(1+\nu')}{17(9+4\nu')}\mu' a, \quad k^{(2)} = \frac{144(1+\nu')}{17(9+4\nu')}\mu' a, \quad k^{(3)} = \frac{96(1+\nu')}{17(9+4\nu')}\mu' a. \tag{36}$$

In eqs. (35) and (36), $\mu'$, $E'$ and $\nu'$ are the shear modulus, Young's modulus and Poisson ratio of simulated material, respectively. Then the network model becomes a simplified spring network model.

Fig. 6 shows the relation between Poisson ratio $\nu'$ and the relative errors of Young's modulus and shear modulus of the simplified spring network model. Obviously, the relative errors are always less than 11%. For most of engineering materials with Poisson ratio between 0.15 and

0.35, the relative errors are less than 5%. The spring network model takes into account both the low-cost and high accuracy.

It has been verified[11,12] that, for engineering short-fiber reinforced composite, the matrix material can be simulated by network cells and the needle-like reinforcers can be represented by 1-D additional long components. In the large-scale analysis, such a discrete manner, shown in fig. 7, greatly reduces the computational cost. Meanwhile, network model is easy to establish the simple and explicit failure criteria of 1-D component by virtue of the physical mechanism of micro-crack defects. Liu et al.[11,12] have successfully investigated the strain distribution regularity in short-fiber reinforced composites.

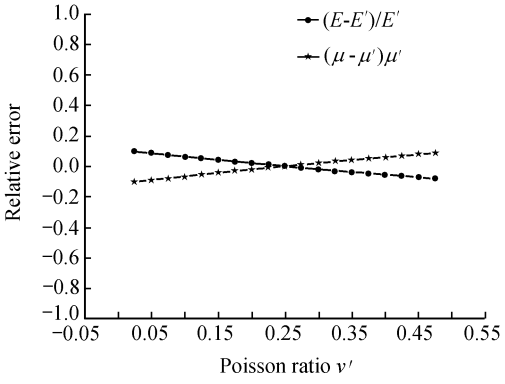


Fig. 6. Relative error of $E$ and $\mu$.

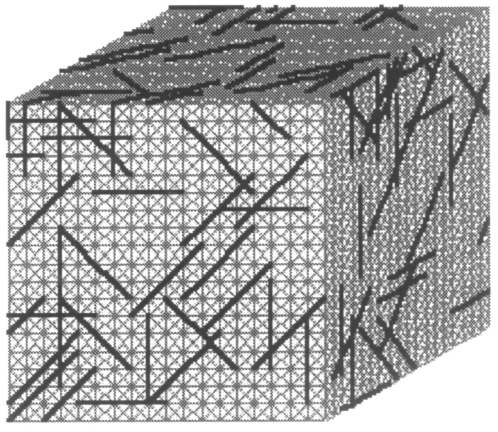

Fig. 7. Simulation of short-fiber reinforced composites.

## 5 Conclusion

(1) Based on the interaction between discrete particles, a material model, whose framework is parallel spring-bundles oriented in the 3-D space, is proposed. The optimum discrete manner is derived, and a 3-D network model composed of 1-D spring components is constructed.

(2) A calibration formulae is derived to determine the geometrical and physical parameters of the 3-D network model which is able to exactly simulate materials with arbitrary Poisson ratio from 0 to 0.5.

(3) The simplification of network model is investigated to realize high computation accuracy within low computation cost. An example shows that such a network model has particular superiority in the simulation of short-fiber reinforced composites.

**Acknowledgements** This work was supported by the National Natural Science Foundation of China (Grant Nos. 19872065 and 19732060), and the project KGCX1-11 supported by the Chinese Academy of Sciences Foundation.

## References

1. Hrennikoff, A., Solution of problem of elasticity by the framework method, J. Appl. Mech., 1941, 12: 169—175.
2. Holnicki-szulc, J., Rogula, D., Nonlocal continuum models of large engineering structures, Arch. Mech., 1979, 31(6): 793—802.

3. Herrmann, H. J., Roux, S., Statistical Models for the Fracture of Disordered Media, Elsevier Science, 1992.
4. Schlangen, E., Garboczi, E. J., Fracture simulations of concrete using lattice models: computation aspects, Eng. Fract. Mech., 1997, 57: 319—332.
5. Curtain, W. A., Scher, H., Brittle fracture in disordered materials: a spring network model, J. Mater. Res., 1990, 5: 535—553.
6. Chiaia, B., Vervuurt, A., van Mier, J. G. M., Lattice model evaluation of progressive failure in disordered particle composites, Eng. Fract. Mech., 1997, 57: 301—318.
7. Murat, M., Anholt, M., Wranger, H. D., Fracture behavior of short-fiber reinforced material, J. Mat. Res., 1992, 7: 3120.
8. Monette, L., Anderson, M. P., Ling, S. et al., Effect of modulus and cohesive energy on critical fiber length in fiber-reinforced composites, J. Mater. Sci., 1992, 27: 4393—4405.
9. Liu, X. Y., Yan, W. D., Liang, N., A pseudo-plastic engagement effect on the toughening of discontinuous fiber-reinforced brittle composites, Metals and Materials, 1998, 4: 242—246.
10. Ostojastarzewski, M., Sheng, P. Y., Alzebdeh, K., Spring network models in elasticity and fracture of composites and polycrystals, Comp. Mater. Sci., 1996, 7: 82—93.
11. Liu, Q. Y., Liang, N., Liu, X. Y., Prediction of mechanical property of whisker reinforced metal matrix composite: part-I Model and Formulation, Chinese Journal of Aeronautics, 2000, 13: 182—187.
12. Liu, X. Y., Liu, Q. Y., Liang, N., Prediction of mechanical property of whisker reinforced metal matrix composite: part-II Verification and Application, Chinese Journal of Aeronautics, 2000, 13: 188—192.